

Modular variable laser cooling for efficient entropy extraction

B. de Neeve,^{1,*} T.-L. Nguyen,^{1,†} A. Ferk,¹ T. Behrle,¹ F. Lancellotti,¹ M. Simoni,¹ S. Welte,^{1,‡} and J. P. Home^{1,2,§}

¹*Institute for Quantum Electronics, ETH Zürich, Otto-Stern-Weg 1, 8093 Zürich, Switzerland*

²*Quantum Center, ETH Zürich, 8093 Zürich, Switzerland*

(Dated: August 30, 2024)

We propose and experimentally demonstrate a method for laser cooling an oscillator based on sequences of spin-state-dependent displacements followed by spin repumping. For a thermal state with mean occupation $\bar{n} \gg 1$ the method attains a reduction to 0.632 of the initial thermal oscillator occupation for two repumps of the two-level spin state. This is within a factor of 2.53 of the optimum that might be expected due to the reduction of the oscillator entropy by $2\ln(2)$. We show that the method, which is based on encoding the value of the modular-variable of the oscillator into the spin, has a simple semi-classical description in terms of a Bayesian update. We demonstrate the method experimentally using the internal and motional states of a single trapped ion.

Laser cooling has been transformative in its effect on atomic physics [1, 2], and the techniques involved have now spread to manufactured opto-mechanical systems [3–5] as well as to molecules [6]. It involves coupling the motional degree of freedom to be cooled to an ancillary system (often the internal states of an atom) which then releases a photon into the low occupancy reservoir of the optical vacuum, transferring entropy into the environment. The purification of a fully mixed two-level spin state results in a reduction of von Neumann entropy corresponding to the value of $\ln(2)$. However, standard methods such as Doppler and sideband cooling, devised based on experimental simplicity, are far from attaining such performance. It is therefore tempting to consider whether cooling techniques approaching this optimal entropy reduction can exist. Such methods could have a considerable advantage over current methods for cooling a highly excited oscillator. For instance, for a thermally occupied oscillator with $\bar{n} \gg 1$ the entropy scales as $\ln(\bar{n})$ and a reduction of $\ln(2)$ results in halving the mean thermal energy.

In this Letter, we propose and demonstrate experimentally a method which, unlike standard cooling methods, reduces entropy in proportion to the fundamental bound given by spin relaxation. It involves two sequential unitary operations which couple the oscillator to an ancillary two-level spin (i.e. qubit), which is then reset. The protocol allows the energy of the thermal oscillator state to be reduced by a factor of 0.632 for each pair of optical pumping events, for any thermal equilibrium state with $\bar{n} \gg 1$. This is a constant factor of 2.53 larger than the ultimate limit of 0.25 energy reduction attainable by two spin resets (removing a maximum entropy of $2\ln(2)$).

The method, which is inspired by recently demonstrated techniques for stabilizing GKP states [7] in superconducting circuits [8] and trapped ions [9], is based on the circuit shown in Fig. 1 a), consisting of two spin-controlled oscillator displacements $U_{CD}(\gamma, \mathcal{P}) \equiv D(\gamma\mathcal{P}) = \exp(2i\mathcal{P}(\text{Im}\{\gamma\}\hat{q} - \text{Re}\{\gamma\}\hat{p}))$ of amplitude $\gamma \in \mathbb{C}$, with sign controlled by the internal state of the spin in the basis of the chosen Pauli operator

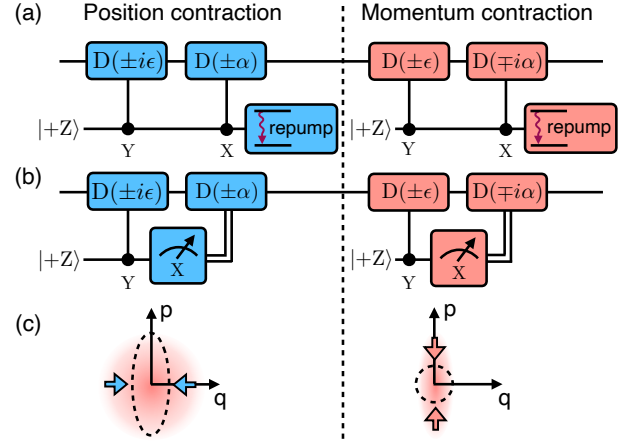


FIG. 1: a) Circuit for a single round of modular-variable cooling of an oscillator. Prior to each qubit reset are two state-dependent displacements in orthogonal directions and with orthogonal spin control bases. The spin basis used for the conditional unitaries is labelled at the control point. This conditions the sign (i.e. direction) of the displacement. b) Circuit which is equivalent in its action on the oscillator (when we average over measurement outcomes), but which involves measurement of the spin and conditional classical feedback. The measurement basis is indicated in the measurement symbol. c) Schematic representation of position and momentum contraction in phase space acting on an initially thermal state shown by its Wigner function.

$\mathcal{P} \in \{X, Y, Z\}$, followed by spin reset by optical pumping. We have defined the dimensionless phase-space position as $\hat{q} \equiv \sqrt{m\omega/(2\hbar)}\hat{q}_r$ and momentum as $\hat{p} \equiv \sqrt{1/(2\hbar\omega m)}\hat{p}_r$ and \hat{q}_r, \hat{p}_r are operators for the real space co-ordinates (for this definition $[\hat{q}, \hat{p}] = i/2$). State-dependent displacements are extensively used in ion-trap physics [10–12], while analogous operations have also recently been realized in superconducting circuits [8]. The first of each pair of operations in Fig. 1

a), which we designate as the *measurement operation*, realizes $U_{\text{CD}}(\epsilon e^{i\theta_m}, Y)$, $\epsilon \in \mathbb{R}$. The second *correction operation*, realizes $U_{\text{CD}}(\alpha e^{i(\theta_m - \pi/2)}, X)$, $\alpha \in \mathbb{R}$, and thus is aligned with the perpendicular quadrature, and acts in the perpendicular spin basis. For the *first* pair of operations in Fig. 1 a), $\theta_m = \pi/2$ and the measurement displacement is aligned with the imaginary phase-space axis, with the corresponding correction a displacement along the real phase-space axis. Following the unitary action, $U_q = U_{\text{CD}}(\alpha, X)U_{\text{CD}}(i\epsilon, Y)$, of these two controlled-displacements, the qubit state is reset by optical pumping. We refer to this as a position contraction. The same sequence is then performed, but with $\theta_m = 0$, realizing a unitary U_p which after reset results in a momentum contraction. Assuming for the moment no effect on the oscillator during qubit reset, and denoting the ± 1 eigenstates of Pauli operators by $|\pm \mathcal{P}\rangle$ the output density matrix for an initial oscillator state ρ_j can be obtained using the Kraus representation as

$$\rho_{j+1} = \sum_{\nu, \mu = \pm} K_{p, \nu} K_{q, \mu} \rho_j K_{q, \mu}^\dagger K_{p, \nu}^\dagger, \quad (1)$$

with the corresponding Kraus operators $K_{q, \pm} \equiv \langle \pm X | U_q | + Z \rangle$

$$K_{q, \pm} = e^{\mp 2i\alpha \hat{p}} \cos(2\epsilon \hat{q} \pm \pi/4). \quad (2)$$

and a similar form obtained from the momentum contraction as $K_{p, \pm} \equiv \langle \pm X | U_p | + Z \rangle$.

To understand the action of this operation on the oscillator state, it is useful to consider the modified sequence of Fig. 1b), which produces the same Kraus map, but involves a modular value measurement followed by conditional feedback [8, 10]. The measurement probabilities are given by $P(\pm X | \rho) = \frac{1}{2}(1 \mp \text{Tr}(\hat{O}\rho))$ with $\hat{O} = \sin(4\epsilon \hat{q})$ and ρ the initial motional density matrix. For an initial position eigenstate satisfying $\hat{q}|q\rangle = q|q\rangle$, we then obtain a conditional probability

$$P(\pm X | q) = \frac{1}{2}(1 \mp \sin(4\epsilon q)). \quad (3)$$

In the Bloch-sphere picture, we can view the spin state prior to the measurement as having been rotated about the Y axis by an angle $-4\epsilon q$. For more general states the spin state will be a superposition corresponding to the distribution of the oscillator in q . The projective spin state measurement result is used to condition the direction of the feedback displacement which should be applied to the oscillator. For cooling this should be chosen such as to move the state towards the phase-space origin on average, as will be explained below.

This interpretation of the quantum mechanical operation in terms of a measurement plus conditional feedback motivates an understanding through the following semi-classical treatment, which assumes the oscillator to be

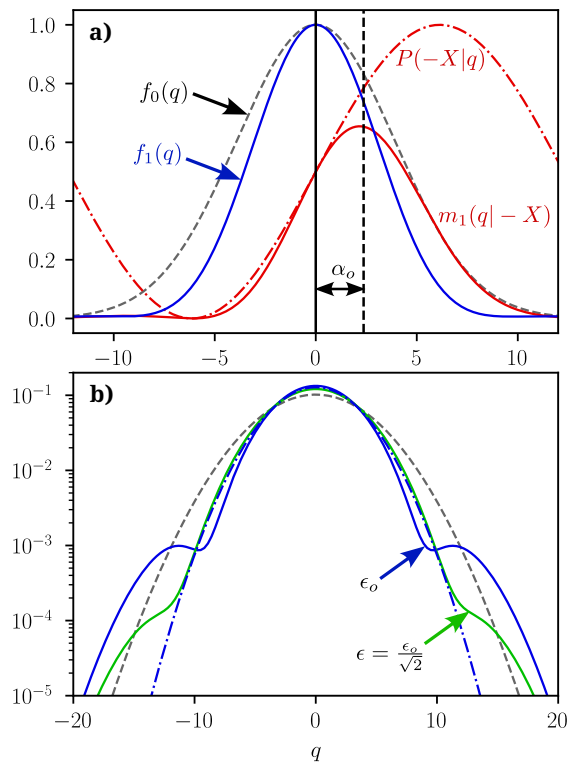


FIG. 2: a) Position contraction in the semi-classical Bayes description. The initial Gaussian probability density (grey dashed curve) is normalized to a peak height of unity. The modular measurement produces a conditional probability $P(-X|q)$ given here for the optimal value ϵ_o (given by the dot-dashed red curve), producing the modified conditional probability $m_1(q|-X)$ (solid red curve) which is close to a Gaussian displaced from the origin by α_o . The narrowed post-correction probability density is $f_1(q)$ (solid blue curve), again normalized to a peak height of 1. b) Probability densities for optimal post-contraction settings (blue solid) and with $\epsilon = \epsilon_o/\sqrt{2}$ (green solid) on a logarithmic scale, emphasizing the deviations from a Gaussian distribution. The latter produces a smaller reduction in the mean energy but reduces the “tails” of the distribution. Additional curves show Gaussian distributions for both the initial temperature (grey dashed), and for the optimal temperature after one round of cooling (blue dot-dashed).

a classical variable and can be understood in terms of a Bayesian update of a probability density. We assume that the initial state is thermal, with a Gaussian joint probability density $w_0(q, p) = f_0(q)f_0(p)$ with $f_0(q) = 1/(s\sqrt{2\pi}) \exp(-q^2/(2s^2))$. For the co-ordinate definitions above, the relation to the thermal occupancy is $s = \sqrt{(\bar{n} + 1/2)}/2$. Let us first consider the reduction in the position quadrature. The modular

variable measurement produces a conditional probability Eq. 3 which allows us to update the probability density of the oscillator according to Bayes rule as $m_1(q|\pm X) \propto P(\pm X|q)f_0(q)$. Fig. 2 a) shows $f_0(q)$, $P(-X|q)$ and $m_1(q|-X)$. For the parameter choice made in this example, $m_1(q|-X)$ approximates a Gaussian distribution which is narrower than $f_0(q)$ with its center displaced from the origin. To recover an approximate thermal distribution, a displacement of the probability density back to the origin is required, which is accomplished by the correction displacement operation $\hat{T}_{\text{class}}(q, -\alpha) : f(q) \mapsto f(q + \alpha)$. Similar logic holds conditioned on the measurement result $+X$, with the opposite sign on the correction displacement. Summing over these two possibilities, the probability density in position becomes $f_1(q) = P(+X)m_1(q - \alpha|+X) + P(-X)m_1(q + \alpha|-X)$. Since the position and momentum are classically independent variables, the same procedure can be repeated using appropriate settings for the momentum quadrature, leading to a final state described classically by $w_1(q, p) = f_1(q)f_1(p)$. The expectation value of the energy for $w_1(q, p)$ is

$$\langle E \rangle_{\text{classical}} = 2\hbar\omega \left(\alpha^2 + s^2 \left(1 - 8\alpha\epsilon e^{-8\epsilon^2 s^2} \right) \right). \quad (4)$$

This expression can be minimized with respect to α, ϵ to find the most effective settings for cooling in the limit where the classical approximation is valid, resulting in the optimal parameter values $\alpha_o = s/\sqrt{\epsilon}$, $\epsilon_o = 1/(4s)$ and a reduction in the energy expectation value by a factor $(e - 1)/e \simeq 0.632$. In Fig. 2 b) we show the phase-space distribution in one quadrature using these values on a log scale, which emphasizes that $w_1(q, p)$ is not an exact Gaussian but is a close approximation. The issue of the residual tails in the distribution will be discussed below.

A more exact result can be obtained from the density matrix ρ_1 obtained from Eq. 1 with ρ_0 a thermal state, giving

$$\langle E \rangle_{\text{quantum}} = \langle E \rangle_{\text{classical}} + 2\hbar\omega \left(\epsilon^2 - \alpha\epsilon e^{-8\epsilon^2 s^2} \left(4s^2 (\cos(4\epsilon^2) - 1) + \sin(4\epsilon^2) \right) \right). \quad (5)$$

where $\langle E \rangle_{\text{classical}}$ is obtained from Eq. 4. Close to the optimal values α_o, ϵ_o the difference between the classical and quantum result is of order $1/s^2$, and is thus a minor correction for $\bar{n} \gg 1$. As the system approaches the ground state, the correction to the classical result becomes more significant, and the optimal parameters deviate from α_o, ϵ_o . Nevertheless, we observe that it is possible to find values of ϵ and α which produce cooling well below $\bar{n} = 1$. For a given value of ϵ the energy $\langle E \rangle_{\text{quantum}}$ is minimized by choosing

$$\alpha = \frac{1}{2} \epsilon e^{-8\epsilon^2 s^2} \left(4s^2 (1 + \cos(4\epsilon^2)) + \sin(4\epsilon^2) \right). \quad (6)$$

We can find the optimal value of ϵ by setting α as in Eq. 6 and minimizing Eq. 5 numerically.

We demonstrate the method using the axial motion of a single trapped $^{40}\text{Ca}^+$ ion with a frequency of around $\omega_m \approx 2\pi \times 1.7$ MHz. The motional mode is controlled and read out via the internal electronic levels $|+Z\rangle_s \equiv |^2S_{1/2}, m_j = 1/2\rangle$ and $|-Z\rangle_s \equiv |^2D_{5/2}, m_j = 3/2\rangle$, separated by a transition at 729 nm, forming the internal-state qubit (where subscript s refers to *spin*). The electronic state is initially prepared in $|+Z\rangle_s$. Then the two state-dependent displacements are implemented by application of a bi-chromatic laser pulse simultaneously driving the red and blue motional sidebands of the qubit transition, realizing the Hamiltonian $\hat{H} = \hbar\eta\Omega\sigma_{\phi_s}(\sin(\phi_m)\hat{q} - \cos(\phi_m)\hat{p})$ with $\sigma_{\phi_s} \equiv (\cos(\phi_s)X + \sin(\phi_s)Y)$ and $\eta \simeq 0.05$ the Lamb-Dicke parameter [13]. The spin phase ϕ_s can be chosen by the mean phase of the two laser drives, and the motional phase ϕ_m by the difference of their phases. Applied for a time period t this realizes $U_{\text{CD}}(\gamma, \mathcal{P})$ with $\gamma(t) = \mp\eta\Omega t e^{i\phi_m}/2$, allowing Ωt and ϕ_m to be used to control $\epsilon, \alpha, \theta_m$, and θ_c . Reset of the qubit is performed by optical pumping, which we estimate requires scattering an average close to 2 photons, one at 854 nm and one at 397 nm [9].

We prepare initial thermal states of the oscillator with \bar{n} of 14.7 ± 0.8 , 34.0 ± 1.8 , and 51.1 ± 4.4 by performing Doppler cooling with selected laser powers and detunings. We characterize the temperature of these initial states by measuring the characteristic function using state-dependent displacements [14], and fitting the obtained data with the Gaussian form expected for a thermally excited oscillator. For each initial state we extract the value of \bar{n} from the width of the Gaussian, which is narrower for larger \bar{n} . At higher occupations, we find that to obtain accurate estimates of the values of \bar{n} , we must include higher order interactions in the Hamiltonian that arise outside the Lamb-Dicke regime [13], including the effects of thermally excited radial modes with approximate frequencies of $2\pi \times 2.4$ MHz and $2\pi \times 3.2$ MHz. The latter modify the coupling rate Ω . Further details on the estimation of \bar{n} from characteristic function readout are given in the Supplemental Material.

We then apply the modular variable cooling for several rounds and subsequently measure the characteristic function of the oscillator, from which we extract \bar{n} as described above for thermal states. The values of α and ϵ at each round were chosen assuming that \bar{n} is reduced by the optimal amount. Unlike the initial states, the cooled states are only approximately thermal and contain high energy ‘‘tails’’, as noted above, but the Gaussian fit allows us to obtain the mean occupation of the ‘‘thermal fraction’’. The values thus obtained are plotted in Fig. 3, along with a comparison to the scaling 0.632^{rounds} as well as numerical simulations which take account of known experimental imperfections. For the

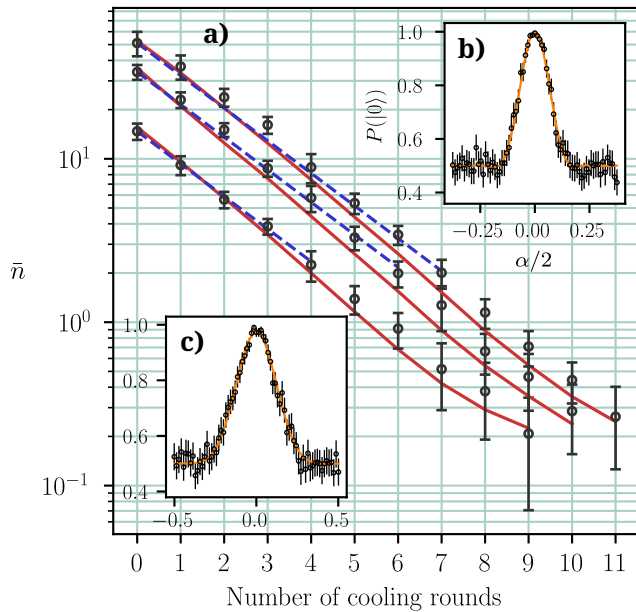


FIG. 3: Estimated values of \bar{n} after each cooling round, starting from initial thermal states prepared with $\bar{n} \approx 15$, 34, and 51. a) Error bars are 95% confidence intervals obtained from Gaussian fits of experimentally measured characteristic functions. The blue dashed lines give $\bar{n}_0 \times 0.632^{\text{rounds}}$ predicted by the semi-classical theory, which due to quantum effects is not expected to be valid for $\bar{n} < 2$. Red lines give \bar{n} predicted by numerical simulations of the experiment including several known imperfections. The insets show fits to characteristic functions readout data for b) an initial state with $\bar{n} \approx 34$ and c) a state after three cooling rounds starting from initial state with $\bar{n} \approx 34$, for which the obtained $\bar{n} \approx 8.5$.

first few rounds of cooling we observe good agreement between the simulation and semi-classical theory. After more rounds the simulation deviates from a thermal state which may explain the colder states predicted compared to the semi-classical theory; although the reduction of \bar{n} of 0.632 predicted by the semi-classical theory makes no thermal assumption on the *final* state after a *single* round, by assuming a 0.632 reduction over many rounds we are implicitly assuming the state is thermal before *each* round of cooling is applied. Thus the values of \bar{n} extracted from the simulation gradually deviate below the semi-classical theory as the high-energy components are increasingly neglected by the semi-classical theory. The results from the experiment mostly agree quite well with the semi-classical theory, but tend to slightly higher values of \bar{n} than the simulation in the early rounds.

The deviation from a thermal state increases with the temperature of the initial thermal state and the number of cooling rounds. After performing many rounds of

cooling, a large fraction of the population reaches the ground state, while some remains in the tails of the distribution at high energy. We quantify the amount of population close to the ground state by performing a blue-sideband pulse after the cooling and looking at the contrast of the resulting Rabi oscillations. We have thus found populations of $\sim 2.6\%$, 7% , and 13% remaining at high energy in the final states after cooling from initial $\bar{n} \approx 15$, 34, and 51 respectively. Further details are given in the Supplemental Material. Theoretically we see (Fig. 2 b)) that using a less optimal value of $\epsilon = \epsilon_o/\sqrt{2}$ for the cooling leads to high energy tails in the resulting final state that are roughly an order of magnitude lower. We have tried this experimentally, but have not observed a notable change in the high energy tails after many rounds of cooling, although the numerical simulations do show a reduction. The reasons for this are unclear – a more detailed discussion is given in the Supplemental Material.

We conclude that the method is particularly effective at cooling high temperature states, but also limited by the occurrence of high energy tails. Our results show that the highest temperature states that can be effectively cooled with an acceptably low population remaining in high energy tails is limited by the noise model of a particular experiment. We expect that for systems with lower noise and the capability to perform higher fidelity coherent operations the method will become particularly attractive, offering the means to remove a large fraction of the oscillator energy with two repumps while keeping the high energy tails in the final state negligible.

It is instructive to compare the modular variable cooling to Doppler cooling, for an analogy can be drawn based on the classical treatment by considering that the conditional excitation probability for the momentum quadrature, $P(\pm Z|p)$ is proportional to the Lorentzian of the resonance of the transition, while for the position quadrature, the conditional probability is flat. Making the assumption that the range of velocities of the initial state is much smaller than the width of the Lorentzian, a slightly naive approach is then to match the linear approximation of the Lorentzian to a linear approximation $P(\pm X|p) = \frac{1}{2}(1 \pm \sin(4\epsilon p)) \approx \frac{1}{2} \pm 2\epsilon p$, which results in $\epsilon = \eta\omega/\Gamma$ with η the Lamb-Dicke parameter $\eta = \sqrt{E_{\text{recoil}}/\hbar\omega}$ and Γ the decay rate of the transition. The correction displacement is given by the recoil of a single photon, thus is also of size η . Using Eq. 4, the average change in energy is then $2\hbar\omega\eta^2 \left(1 - 2(\nu/\Gamma)(2\bar{n} + 1)e^{-2\eta^2\nu^2(2\bar{n}+1)/\Gamma^2}\right)$. For values such that the exponential factor can be approximated as 1 (Lamb-Dicke and weak-binding regimes [15]) this change is zero for $\bar{n} + 1/2 = \Gamma/(4\omega)$ which is what would be expected as the Doppler limit of the standard theory neglecting the recoil in spontaneous emission [16]. Further details are given in the Supplemental Material. For high \bar{n} , Doppler cooling produces a

fractional reduction in energy which is far from optimal, but it is robust and fast because both the gradient and the measurement correction are far lower than the optimal values found above and the rate of scattering is very high.

The method demonstrated here achieves a reduction in the mean vibrational quantum number by a factor of 0.632 for a single round, which requires two spin resets. Fundamental considerations would imply that the possible reduction in entropy from two spin resets is $2\ln(2)$. An oscillator thermal state has an entropy of $-\bar{n}\ln(\bar{n}/(\bar{n}+1)) + \ln(\bar{n}+1)$, which for $\bar{n} \gg 1$ simplifies to $S_{\text{th}} \simeq \ln(\bar{n})$. Subtracting the entropy from two spin resets then leaves a result $S'_{\text{th}} \simeq \ln(\bar{n}/4)$, which is consistent with reduction of \bar{n} by a factor of 4. This implies that in the limit $\bar{n} \gg 1$ an improvement of up to $4 \times 0.632 = 2.53$ might be achievable by further optimization of the pulse sequence used to implement the cooling, which should form the focus of future investigation. The methods here could be generalized to other states and platforms. The similarity to the earlier work on the stabilization of grid states indicates sequences similar to those given above could be used to cool into highly non-classical states [8, 9]. These first examples point to new possibilities for quantum state generation and control. Due to the appearance of similar Hamiltonians, we expect that these methods will find application in systems beyond trapped ions and atoms, including superconducting circuits and nano-mechanical oscillators.

JH devised the scheme and JH and BN performed the theoretical study. BN, TL, SW, and TB carried out the experiments, and AF developed some required control system features and helped BN to implement the cooling sequence. BN and TL performed numerical simulations. Experimental assistance was provided by FL and MS. The paper was written by JH, BN and SW with input from all authors.

We thank P. Campagne-Ibarcq for stimulating discussions. We acknowledge support from the Swiss National Science Foundation through the National Centre of Competence in Research for Quantum Science and Technology (QSIT) grant 51NF40-160591, and from the Swiss National Science Foundation under grant number 200020 165555/1. S.W. acknowledges financial support via the SNSF Swiss Postdoctoral Fellowship (Project no. TMPFP2_210584).

* Email: brennan.mn@proton.me

† Current address: QuantX Labs Pty Ltd, Adelaide, Australia

‡ Email: stephan.welte@pi5.uni-stuttgart.de; Current address: 5. Physikalisches Institut and Carl-Zeiss-Stiftung Center for Quantum Photonics Jena - Stuttgart

- Ulm, Universität Stuttgart, Pfaffenwaldring 57, 70569 Stuttgart, Germany

§ Corresponding author, Email: jhome@phys.ethz.ch

- [1] D. J. Wineland, R. E. Drullinger, and F. L. Walls, Radiation-pressure cooling of bound resonant absorbers, *Physical Review Letters* **40**, 1639 (1978).
- [2] W. D. Phillips, Nobel lecture: Laser cooling and trapping of neutral atoms, *Reviews of Modern Physics* **70**, 721 (1998).
- [3] J. Chan, T. P. M. Alegre, A. H. Safavi-Naeini, J. T. Hill, A. Krause, S. Gröblacher, M. Aspelmeyer, and O. Painter, Laser cooling of a nanomechanical oscillator into its quantum ground state, *Nature* **478**, 89 (2011).
- [4] U. Delić, M. Reisenbauer, K. Dare, D. Grass, V. Vuletić, N. Kiesel, and M. Aspelmeyer, Cooling of a levitated nanoparticle to the motional quantum ground state, *Science* **367**, 892 (2020).
- [5] M. Aspelmeyer, T. J. Kippenberg, and F. Marquardt, Cavity optomechanics, *Rev. Mod. Phys.* **86**, 1391 (2014).
- [6] E. S. Shuman, J. F. Barry, and D. DeMille, Laser cooling of a diatomic molecule, *Nature* **467**, 820 (2010).
- [7] D. Gottesman, A. Kitaev, and J. Preskill, Encoding a qubit in an oscillator, *Phys. Rev. A* **64**, 012310 (2001).
- [8] P. Campagne-Ibarcq, A. Eickbusch, S. Touzard, E. Zalsgeller, N. E. Frattini, V. V. Sivak, P. Reinhold, S. Puri, S. Shankar, R. J. Schoelkopf, L. Frunzio, M. Mirrahimi, and M. H. Devoret, Quantum error correction of a qubit encoded in grid states of an oscillator, *Nature* **584**, 368 (2020).
- [9] B. de Neeve, T.-L. Nguyen, T. Behrle, and J. P. Home, Error correction of a logical grid state qubit by dissipative pumping, *Nature Physics* **18**, 296 (2022).
- [10] C. Flühmann, V. Negnevitsky, M. Marinelli, and J. P. Home, Sequential modular position and momentum measurements of a trapped ion mechanical oscillator, *Phys. Rev. X* **8**, 021001 (2018).
- [11] H.-Y. Lo, D. Kienzler, L. de Clercq, M. Marinelli, V. Negnevitsky, B. C. Keitch, and J. P. Home, Spin-motion entanglement and state diagnosis with squeezed oscillator wavepackets, *Nature* **521**, 336 (2015).
- [12] J. Benhelm, G. Kirchmair, C. F. Roos, and R. Blatt, Towards fault-tolerant quantum computing with trapped ions, *Nature Physics* **4**, 463 (2008).
- [13] D. J. Wineland, C. Monroe, W. M. Itano, D. Leibfried, B. E. King, and D. M. Meekhof, Experimental issues in coherent quantum-state manipulation of trapped atomic ions, *J. Res. Natl. Inst. Stand. Technol.* **103**, 259 (1998).
- [14] C. Flühmann and J. P. Home, Direct characteristic-function tomography of quantum states of the trapped-ion motional oscillator, *Phys. Rev. Lett.* **125**, 043602 (2020).
- [15] D. J. Wineland and W. M. Itano, Laser cooling of atoms, *Phys. Rev. A* **20**, 1521 (1979).
- [16] D. Leibfried, R. Blatt, C. Monroe, and D. Wineland, Quantum dynamics of single trapped ions, *Rev. Mod. Phys.* **75**, 281 (2003).
- [17] K. E. Cahill and R. J. Glauber, Ordered expansions in boson amplitude operators, *Phys. Rev.* **177**, 1857 (1969).
- [18] S. M. Barnett and P. M. Radmore, *Methods in Theoretical Quantum Optics* (Oxford University Press, 2002).
- [19] R. Loudon, *The Quantum Theory of Light*, 3rd ed. (Oxford University Press, Great Clarendon Street, Oxford OX2 6DP, 2000).

Supplemental Material: Modular variable laser cooling for efficient entropy extraction

B. de Neeve,^{1,*} T.-L. Nguyen,^{1,†} A. Ferk,¹ T. Behrle,¹ F. Lancellotti,¹ M. Simoni,¹ S. Welte,^{1,‡} and J. P. Home^{1,2,§}

¹*Institute for Quantum Electronics, ETH Zürich, Otto-Stern-Weg 1, 8093 Zürich, Switzerland*

²*Quantum Center, ETH Zürich, 8093 Zürich, Switzerland*

(Dated: August 30, 2024)

QUANTUM TREATMENT OF COOLING PROCESS

Calculations of the update to the energy following a single round of cooling were performed using the normal ordered characteristic function, which is defined for the density matrix ρ as

$$\chi(\beta) = \text{Tr}(D(\beta)\rho) e^{|\beta|^2/2}. \quad (\text{S.1})$$

The relevant density matrix is given by ρ_1 in Eq. 1 in the main manuscript, which consists of a sum of 16 terms weighted by $1/16$ with a complex amplitude $c_{\gamma,\chi}$, each of which constitutes a displacement on the left (right) by a particular value γ (χ) of the original thermal density matrix $\rho_0 = \sum_n p_n |n\rangle\langle n|$, with $|n\rangle$ the energy eigenstates, and $p_n = \bar{n}^n / (\bar{n} + 1)^{n+1}$ the relevant probabilities for a thermal distribution. The result for the characteristic function is a sum of terms

$$\chi_{\rho_1}(\beta) = \frac{e^{|\beta|^2/2}}{16} \sum_{\{\gamma,\chi\}} c_{\gamma,\chi} \sum_n p_n \text{Tr}(D(\beta)D(\chi)|n\rangle\langle n|D(-\gamma)) \quad (\text{S.2})$$

which using the cyclic property of the trace gives

$$\chi_{\rho_1}(\beta) = \frac{e^{|\beta|^2/2}}{16} \sum_{\{\Upsilon\}} c_{\gamma,\chi} \sum_n p_n \langle n|D(\Upsilon)|n\rangle, \quad (\text{S.3})$$

where $D(\Upsilon) = D(-\gamma)D(\beta)D(\chi)$. The sum over a thermal distribution of the diagonal elements of a displacement operator in the energy eigenbasis [17] then gives

$$\chi_{\rho_1}(\beta) = \sum_{\Upsilon} e^{-|\Upsilon|^2 \bar{n}}. \quad (\text{S.4})$$

The mean occupation can be found from the characteristic function using

$$\langle n \rangle = - \left. \frac{\partial^2}{\partial \beta \partial \beta^*} \chi_{\rho_1}(\beta) \right|_{\beta=0}. \quad (\text{S.5})$$

CHARACTERISTIC FUNCTION READOUT

We estimate the values of \bar{n} of initial thermal states in the experiment as well as approximate thermal states after cooling by applying a state-dependent displacement

$D(\alpha X/2)$. Given an oscillator state density matrix ρ the measurement probability of the spin is then

$$P(|+Z\rangle) = \frac{1}{2} (1 + \text{Re}\{\langle D(\alpha) \rangle\}), \quad (\text{S.6})$$

allowing to determine the real part of $\langle D(\alpha) \rangle$, which is the symmetric ordered characteristic function [18]. One may also measure the imaginary part of the characteristic function by performing an appropriate single-qubit rotation before the measurement [14]. We do not do this because the characteristic function for thermal states is real-valued. The Hamiltonian

$$\hat{H} = \hbar \eta \Omega \sigma_{\phi_s} (\sin(\phi_m) \hat{q} - \cos(\phi_m) \hat{p}) \quad (\text{S.7})$$

(where $\sigma_{\phi_s} \equiv (\cos(\phi_s)X + \sin(\phi_s)Y)$ and $\eta \simeq 0.05$ is the Lamb-Dicke parameter) that is used to realise the state-dependent displacement $D(\alpha X/2)$ is only the lowest order term of the Lamb-Dicke expansion [13], and for highly excited thermal states we fit the readout data using a simulation that models the full expansion. In addition, since the radial modes are expected to also be in thermal states we must account for their effect, which is to modify the effective Rabi rate Ω in Eq. S.7 dependent on the occupancy of the radial modes. In particular, if each of the two radial modes are in energy eigenstates $|n_1\rangle, |n_2\rangle$, then the effective Rabi frequency of the drive is

$$\Omega \prod_{j=1,2} e^{-|n_j|^2/2} L_{n_j}(|\eta_j|^2), \quad (\text{S.8})$$

where $L_n(x)$ are Laguerre polynomials. For the experiments we performed the radial mode frequencies were $\omega_1 \simeq 2\pi \times 2.4$ MHz, $\omega_2 \simeq 2\pi \times 3.2$ MHz, and the Lamb-Dicke parameters $\eta_1 \simeq 0.02$, $\eta_2 \simeq 0.03$. For a thermal state the probability of radial mode occupancy n_j is $P_{n_j} = \bar{n}_j^{n_j} / (\bar{n}_j + 1)^{n_j+1}$, leading to a *distribution* of Rabi frequencies given by Eq. S.8. We model the effect by a simulation that samples the Rabi frequency from the thermal distribution for each radial mode. We then repeat and average the result of the simulation over many samples. The values of \bar{n}_j are estimated assuming each mode to reach the same temperature in the steady-state of Doppler cooling. In Fig. S.1 we show an example plot of characteristic function readout data for an initially prepared thermal state with $\bar{n} \approx 51$ in the axial mode with a fit that uses the described model. If the readout probabilities were

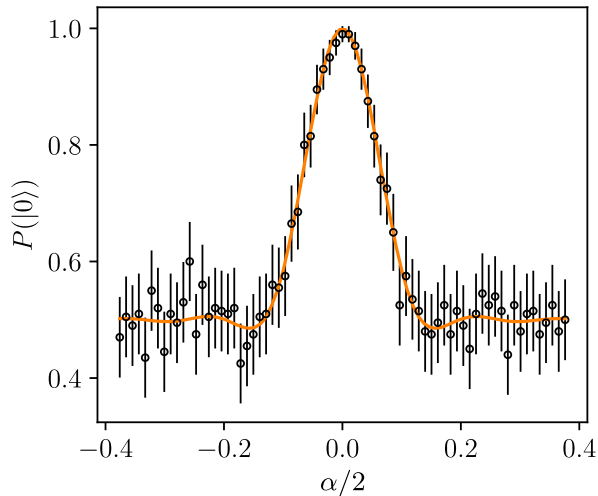


FIG. S.1: Characteristic function readout of a thermal state with $\bar{n} \approx 51$ (highest \bar{n} initial state in Fig. 3 of the main text). The lowest order term in the Lamb-Dicke expansion would lead to readout probabilities given by Eq. S.6 which is a Gaussian function for thermal states. The non-Gaussian features are due to higher order terms in the Lamb-Dicke expansion. Each data point is the average over 200 experimental shots. Error bars are 95 % confidence intervals of binomial errors.

given simply by Eq. S.6, the functional form would be Gaussian, however the higher order terms in the Lamb-Dicke expansion lead to non-Gaussian features seen in the figure as small oscillations in addition to the overall Gaussian form expected from a thermal characteristic function. In Fig. S.2 we plot experimentally measured characteristic function readout data corresponding to the curve in centre of Fig. 3 a), starting from an initial thermal state with $\bar{n} \approx 34$. The symmetric ordered characteristic function of the initial thermal state is a narrow Gaussian, and as the state of the oscillator is cooled the resulting approximate thermal state has an approximately Gaussian characteristic function which is broader than the initial state. After 10 rounds of cooling most of the population reaches the ground state having a characteristic function with a large variance (the symmetric ordered characteristic function is the two-dimensional Fourier transform of the Wigner function [18]).

NUMERICAL SIMULATION

In Fig. 3 of the main text we have plotted \bar{n} estimates obtained from numerical simulations of the cooling process. For these simulations the state of the spin and oscillator systems is represented by a density matrix,

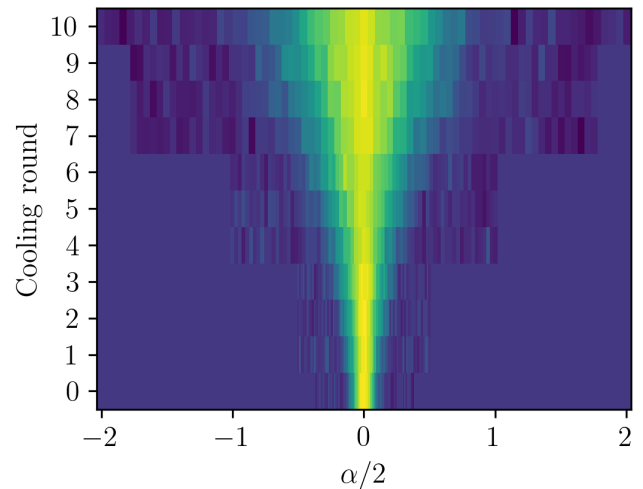


FIG. S.2: Characteristic function readouts for an initial thermal state with $\bar{n} \approx 34$ and after each of 10 cooling rounds, corresponding to the intermediate temperature data plotted in Fig. 3 of the main text. The central peak reaches $P(|+Z\rangle) = 1$ and the probability $P(|+Z\rangle)$ drops to $\sim 1/2$ for large values of α . Each point is the average of 400 experimental shots.

where the oscillator Hilbert space is truncated in the energy eigenbasis. Both effects mentioned above to estimate \bar{n} from characteristic function readouts, namely higher order terms in the Lamb-Dicke expansion and the effects of thermally excited radial modes have been included in these simulations as well. In addition we have modelled Markovian noise including

- Spin dephasing with collapse operator Z .
- Oscillator dephasing with collapse operator $a^\dagger a$.
- Oscillator heating with collapse operator a^\dagger .

For the spin dephasing we have modelled some non-Markovian noise as well using a term in the Master equation of the form

$$\frac{d\rho}{dt} = \frac{g^2}{K} (e^{-Kt} - 1) [Z, [Z, \rho]], \quad (\text{S.9})$$

which models both Gaussian (non-Markovian) and exponential (Markovian) decay to better approximate what we have measured in the experiment. For the spin dephasing we have used $g = 1/1.6$ kHz, and $K = 1/5$ kHz to model a coherence time of ~ 1.6 ms measured experimentally with a similar component of Gaussian decay. For the oscillator dephasing we have modelled mainly Markovian dephasing with an overall coherence time of ~ 15 ms as measured in the experiment, and we model purely Markovian oscillator heating at a rate of 10 quanta per second.

We model photon recoil due to the repump operations as random displacements sampled from a distribution taking into account the beam geometry and dipole emission pattern. The random displacements are applied to the component of the spin-oscillator state that is in the excited state $| -Z \rangle_s$ while the component in $| +Z \rangle_s$ is left unchanged.

We also model 50 Hz (and higher harmonics) oscillations of the frequency of the axial mode of ion motion that were measured experimentally. Further details can be found in the Methods of ref. [9]. We also simulate a small amount of Gaussian random fluctuations on the axial mode frequency with a standard deviation of 20 Hz.

We observe fluctuations in the temperature of the initial state over the timescales of our measurements. Since we run many trajectories of the Master equation evolution in our simulations in order to sample radial mode occupancies, we can sample other parameters with no additional computational cost. We thus model fluctuations of the temperature of the initial state by sampling a Gaussian distribution of initial \bar{n} values for the initial thermal state. We have set the standard deviation in \bar{n} of the distribution from 2 for lower temperature initial state ($\bar{n} \approx 15$) up to 3 for higher temperature states ($\bar{n} \approx 51$). Similarly, we model fluctuations in calibrated laser pulse parameters: Rabi frequency, and laser detuning from the internal ion qubit transition by sampling Gaussian distributions for these parameters for each trajectory.

HIGH ENERGY TAILS

As shown graphically in Fig. 2 b) of the main text we expect that after performing a round of cooling on an initially thermal oscillator state, the final state is only approximately thermal and contains tails in the position and momentum distribution of the state. When performing further rounds of cooling we expect that the tails remaining from each round accumulate. Thus, after many rounds of cooling a large fraction of the population reaches the ground state while a small fraction remains at higher energy. We expect the fractional amount of population at higher energy in the final state as well as the energy of this population to increase with the temperature of the initial thermal state, before cooling is applied.

To measure this effect we apply a blue-sideband pulse on the final cooled state after many rounds of cooling and measure the internal ion qubit state. For a general oscillator state $\rho = \sum_{j,k} \rho_{jk} |j\rangle_m \langle k|_m$, where $|n\rangle_m$ are the oscillator energy eigenstates, the probability to measure the internal qubit state $|+Z\rangle_s$ after a blue-sideband pulse of duration t on an initial state

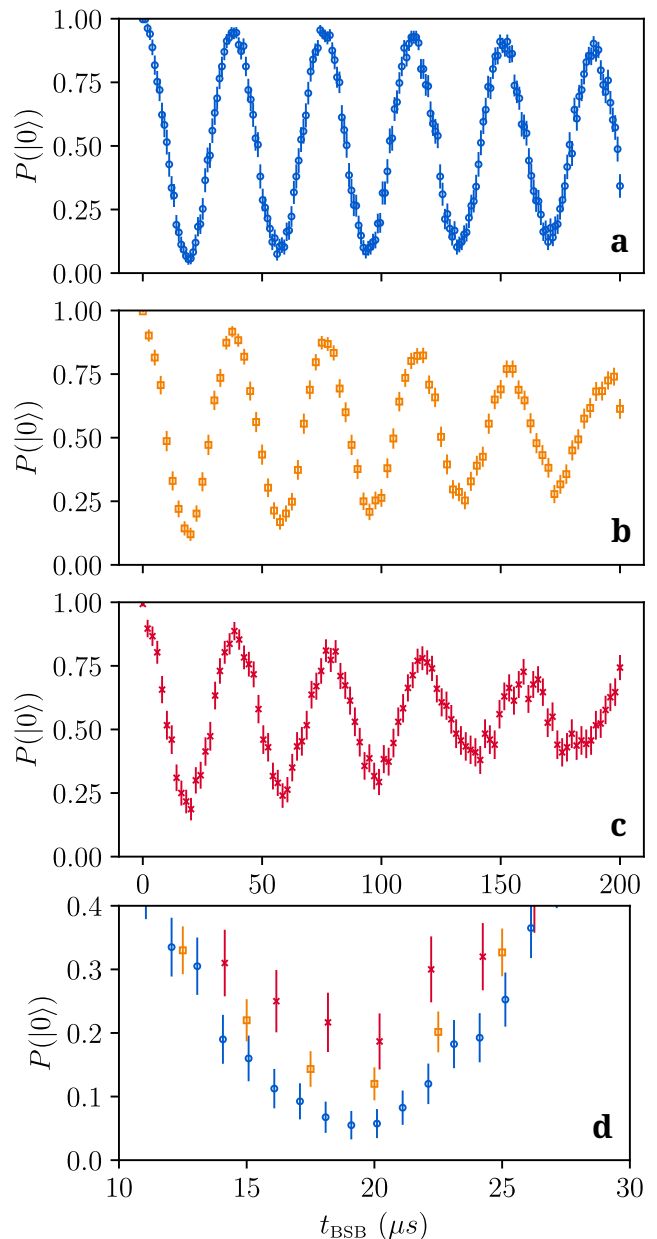


FIG. S.3: Blue-sideband oscillations after cooling. (a) A blue-sideband pulse is applied after 16 rounds of cooling have been performed on an initial thermal state with $\bar{n} \approx 15$. The blue-sideband pulse is followed by measuring the internal state of the ion by fluorescence detection. (b) Same as in (a) but after 17 rounds of cooling on an initial thermal state with $\bar{n} \approx 34$. (c) Same as in (a) but after 16 rounds of cooling on an initial thermal state with $\bar{n} \approx 51$. The plotted values are averages over 400 (a), 600 (b), 300 (c) experimental shots. Each plotted oscillation (a), (b), (c) corresponds to the cooling datasets plotted in Fig. 3 of the main text. (d) Zoomed-in view with combined data from (a), (b), and (c) showing the first minima in the blue-sideband oscillations.

$|+Z\rangle_s \langle +Z|_s \otimes \rho$ is [16]

$$P_0(t) = \frac{1}{2} \left(1 + \sum_{n=0}^{\infty} \rho_{nn} \cos(\Omega_{n,n+1}t) \right), \quad (\text{S.10})$$

where $\Omega_{n,n+1}$ are the Rabi frequencies of the blue-sideband interaction for the transition between states $|+Z\rangle_s |n\rangle_m \leftrightarrow |-Z\rangle_s |n+1\rangle_m$. In the Lamb-Dicke regime (for our experiments this requires $n < \sim 15$), $\Omega_{n,n+1}$ scales as $\sqrt{n+1}$. Thus we expect that the fraction of population in the ground state leads to a sinusoidal oscillation of $P_0(t)$ while the tails at much higher energies lead to a collection of higher frequency oscillations that quickly average out to 1/2, thereby reducing the contrast of the oscillation due to the ground state population. The larger the fraction of population in the high energy tails, the lower the contrast of the oscillation. In Fig. S.3 we plot data measured after performing blue-sideband pulses of varying duration, t_{BSB} , after each of the cooling sequences plotted in Fig. 3. We observe a sinusoidal oscillation due to ground state population and a reduction of contrast as the temperature of the initial thermal state before cooling increases. The rate of decay of the oscillations also increases as the initial state temperature increases. This is expected due to the increasing temperature of the radial modes, which have not been cooled, but whose temperature increases proportionally to that of the initial state in the axial mode (which we have cooled). As the temperature of the radial modes increases there is a broader distribution of energies leading to a broader range of effective Rabi frequencies as given by Eq. S.8, leading to a faster decay of the oscillations plotted in Fig. S.3 as the temperature of the initial state is increased.

To estimate the fraction of population remaining in the tails of the Fock-state distribution we fit a model that allows for exponential and Gaussian decay of the oscillations given by Eq. S.10. When starting the cooling from thermal states with $\bar{n} \approx 15$ and 34, we extract a total population of 0.974 ± 0.026 and 0.929 ± 0.047 respectively in the subspace spanned by $|0\rangle_m$ and $|1\rangle_m$ and find negligible population estimates for Fock states $|n\rangle_m$, $n > 1$. After cooling from an initial thermal state with $\bar{n} \approx 51$ we find a total population of 0.873 ± 0.177 in Fock states with $n < 4$ and negligible populations in higher levels. Thus, for the three datasets starting from thermal states with $\bar{n} \approx 15, 34, 51$ we estimate high energy tails with populations of $\sim 0.026, 0.07,$ and $0.13,$ respectively.

Although we observe high energy tails in the final state density matrices of the simulations described above, we were unable to precisely predict the populations estimated for the experiments using these simulations, which predict lower tail populations. Furthermore, our simulations show that the tail populations can be reduced

even in the presence of all noise and imperfections simulated by performing slower cooling using larger values of ϵ than optimal (see main text Fig. 2 b)) and performing more cooling rounds. We have tried this in the experiment, but have not observed a significant change in tail populations. Therefore, we conclude that the noise model of the simulation is incomplete with respect to the experiments we have performed, and further study would be required to fully understand the causes affecting tail populations in these particular experiments. However, our simulations also demonstrate that for any experiments well-described by the noise models we *have* simulated, it is possible to achieve much lower tail populations by performing somewhat slower cooling with more rounds.

DOPPLER COOLING THEORY

During Doppler cooling a drive laser excites a dipole allowed transition that decays in a timescale $1/\Gamma$ due to spontaneous emission. For a drive with well-defined frequency ν and atomic transition with frequency ν_0 , the probability of exciting the ion with (dimensionless) momentum p , initially in the ground state, after some time t , is given by [16, 19]

$$P(-Z|p) = \frac{1}{\mathcal{N}} \frac{1}{\Gamma^2 + 4(\Delta - 2\eta\omega p)^2}, \quad (\text{S.11})$$

where $\Delta = \nu - \nu_0$, $\eta = \sqrt{\frac{\hbar k^2}{2m\omega}}$ is the Lamb-Dicke parameter, k is the laser wavevector $2\pi/\lambda$ in the direction of the ion motion, m the ion mass, ω is the angular frequency of the ion motional harmonic oscillator mode being cooled, and \mathcal{N} is a normalisation constant to be determined.

Close to the Doppler cooling limit we assume the amplitude of ion motion is small so that the range of momentum p over which the initial state probability is non-negligible is such that the range of $4\eta\omega p$ is narrow compared to the natural linewidth of the transition, Γ . In this case we can approximate $P(-Z|p)$ as a linear function in p (i.e. the Taylor expansion around $p = 0$):

$$P(-Z|p) \approx \frac{1}{\mathcal{N}} \frac{1}{\Gamma^2 + 4\Delta^2} \left(1 + \frac{16\Delta}{\Gamma^2 + 4\Delta^2} \eta\omega p \right). \quad (\text{S.12})$$

Given an ion with an initial thermal (i.e. Gaussian) distribution of momentum

$$f(p) = \frac{1}{\sqrt{2\pi}s} e^{-p^2/2s^2}, \quad (\text{S.13})$$

where $s = \sqrt{(\bar{n} + 1/2)/2}$, we expect the constant \mathcal{N} to be time-dependent such that the probability $P(-Z|p)$ increases over time, since the last emission. On average, a photon will be absorbed after a time τ such that the

probability of detecting the ion in the excited state, $P(-Z) \equiv P_e$. We can solve for the value of \mathcal{N} that satisfies this assumption, i.e.

$$\int_{-\infty}^{\infty} P(-Z|p)f(p)dp = P(-Z) = P_e, \quad (\text{S.14})$$

and using the linear approximation, Eq. S.12, implies

$$\frac{1}{\mathcal{N}} = P_e (\Gamma^2 + 4\Delta^2). \quad (\text{S.15})$$

Then we have

$$P(-Z|p) \approx P_e \left(1 + \frac{16\Delta}{\Gamma^2 + 4\Delta^2} \eta \omega p \right). \quad (\text{S.16})$$

We can obtain an approximation of the energy after absorption and emission of a photon using the semi-classical theory we have used to obtain Eq. 4 in the main text, but using Eq. S.16. That is, we assume an initially thermal state with Gaussian probability density $w_0(q, p) = f(q)f(p)$ where we denote $f(x) = e^{-x^2/(2s^2)}/(\sqrt{2\pi}s)$, and $s = \sqrt{(\bar{n} + 1/2)/2}$ as above. Neglecting the effect of spontaneous emission on the motion, the semi-classical theory predicts a final probability density given by

$$w_1(q, p) = f(q) \left(P(+Z|p)f(p) + P(-Z|p - \eta)f(p - \eta) \right), \quad (\text{S.17})$$

where $P(+Z|p) = 1 - P(-Z|p)$. The shift by η for outcome $-Z$ is due to the momentum transfer to the ion in photon absorption. No shift occurs in the absence of photon absorption ($+Z$ outcome). The expected energy after a chosen time interval (which determines the value of P_e) is

$$\begin{aligned} \langle E \rangle &= \hbar\omega \int_{-\infty}^{\infty} \int_{-\infty}^{\infty} w_1(q, p) (q^2 + p^2) dq dp \\ &= 2\hbar\omega \left(\frac{1}{2} P_e \eta^2 + s^2 \left(1 + P_e \eta^2 \frac{16\omega\Delta}{\Gamma^2 + 4\Delta^2} \right) \right). \end{aligned} \quad (\text{S.18})$$

In the theory above we have not specified the probability of excitation P_e . If we assume a constant drive field amplitude, we might expect a constant probability δP per time step δt since the last absorption-emission (at which point we know the ion is in the ground state). i.e. the probability of excitation in a time δt since the last emission is δP , and the probability of excitation in a time window from $(N-1)\delta t$ to $N\delta t$ is $(1-\delta P)^{N-1}\delta P$, where N is a positive integer. In this case the probability density of excitation per unit time since the last emission is of the form $f_e(t) = \frac{1}{\tau} e^{-t/\tau}$. The average time between absorption events is $\tau = \int_0^{\infty} f_e(t) dt$ and the average probability of excitation is

$$P_e = \int_0^{\tau} f_e(t) dt = \frac{e-1}{e}. \quad (\text{S.19})$$

Knowing the average time τ between absorption events, we could use Eq. S.18 with Eq. S.19 to estimate the average cooling rate. Here we are mainly interested in calculating the minimum attainable energy for which it happens that the value of P_e chosen for the calculation is irrelevant, as we now show.

Setting the final energy equal to the initial energy to find the steady-state energy, i.e. $\langle E \rangle = 2\hbar\omega s^2$, we obtain (the factors of P_e drop out)

$$\bar{n} + \frac{1}{2} = 2s^2 = - \left(\frac{\Gamma^2 + 4\Delta^2}{16\omega\Delta} \right). \quad (\text{S.20})$$

As in the standard Doppler cooling theory [16], the energy is minimised by a detuning $\Delta = -\Gamma/2$. This predicts a minimum energy corresponding to

$$\bar{n} + \frac{1}{2} = \frac{\Gamma}{4\omega}. \quad (\text{S.21})$$

We can relate the linear approximation of $P(\pm Z|p)$ to a linear approximation of $P(\pm X|p)$ from the modular variable cooling theory, i.e.

$$P(\pm X|p) = P_e (1 \pm \sin(4\epsilon p)) \approx P_e (1 \pm 4\epsilon p), \quad (\text{S.22})$$

where $P_e = 1/2$ (see also Eq. 3 in the main text). Using $P_e = 1/2$ in Eq. S.16 and Eq. S.22 matches the offsets. We can then match the slope in Eq. S.22 with that in Eq. S.16 by choosing

$$\epsilon = - \frac{4\eta\omega\Delta}{\Gamma^2 + 4\Delta^2}. \quad (\text{S.23})$$

Assuming $\epsilon^2 s^2 \ll 1$, the energy predicted by Eq. 4 with ϵ given by Eq. S.23 and $\alpha = \eta$ is approximately

$$\langle E \rangle_{\text{classical}} \approx 2\hbar\omega \left(\eta^2 + s^2 \left(1 + \eta^2 \frac{32\omega\Delta}{\Gamma^2 + 4\Delta^2} \right) \right). \quad (\text{S.24})$$

As before, the cooling reaches a steady-state when the change in energy is zero, i.e. $\langle E \rangle_{\text{classical}} = 2\hbar\omega s^2$, which leads to Eq. S.20. Thus Eq. S.24 predicts the same minimum steady-state energy as Eq. S.21.

The Doppler limit expected from the standard theory for Doppler cooling, including fluctuations due to photon absorption at different phases of the ion motion, but neglecting the fluctuations due to spontaneous emission, is given by a temperature [16]

$$T_{\min} = \frac{\hbar\Gamma}{4k_B}, \quad (\text{S.25})$$

where k_B is the Boltzmann constant. For a harmonic oscillator thermal state [18]

$$\bar{n} = \frac{1}{e^{\hbar\omega/k_B T} - 1}. \quad (\text{S.26})$$

When $\hbar\omega \ll k_B T$, we have

$$\bar{n}_{\min} \approx \frac{k_B T_{\min}}{\hbar\omega} = \frac{\Gamma}{4\omega}, \quad (\text{S.27})$$

which matches Eq. S.21 in the classical limit of the

oscillator state (i.e. $\bar{n} \approx \bar{n} + 1/2$; in any case the theory to reach Eq. S.21 assumes classical states).